Songklanakarin J. Sci. Technol.
34 (1), 77-91, Jan. - Feb. 2012

SJST SONGKLANAKARIN JOURNAL OF SCIENCE AND TECHNOLOGY
http://www.sjst.psu.ac.th

Original Article

Projection of bootstrap current in the ITER with standard type I ELMy *H*-mode and steady state scenarios

Yutthapong Pianroj and Thawatchai Onjun*

School of Manufacturing Systems and Mechanical Engineering,
Sirindhorn International Institute of Technology, Thammasat University, Rangsit, Pathum Thani,12121 Thailand.

Received 28 July 2011; Accepted 26 December 2011

Abstract

The investigation of bootstrap current formation in ITER is carried out using BALDUR integrated predictive modeling code. The combination of Mixed B/gB anomalous transport model and NLCASS module together with the pedestal model is used in BALDUR code to simulate the time evolution of temperature, density, and plasma current profiles. It was found in the simulations that without the presence of ITB, a minimal fraction of bootstrap current (as well as low fusion performance) was achieved. The enhancement due to ITB depends sensitively on the strength of toroidal velocity. A sensitivity study was also carried out to optimize the bootstrap current fraction and plasma performance. It was found that the bootstrap current fraction slightly improved; while the plasma performance greatly improved with increasing of NBI power or pedestal temperature. On the other hand, higher impurity concentration resulted in a significant degradation of fusion performance, but a smaller degradation in bootstrap current.

Keywords: ITER, bootstrap current, BALDUR, fusion performance, transport

1. Introduction

Recently, magnetically-confined thermonuclear fusion has received much attention as a potential environmentally-benign power generation mechanism. However, its technical and engineering feasibility has yet to be demonstrated. Consequently, an international project called the International Thermonuclear Experimental Reactor (ITER) was officially initiated in 2006 (Kaname, 2010). Besides the goal of ITER to demonstrate a large-scale production of nuclear fusion power, a non-inductive current for a long pulse operation is also one of its primary targets. The formation of the non-inductive current to reduce or completely replace an inductive current is a crucial issue for the operation of nuclear fusion reactors in the future. It is widely accepted that the non-inductive current can be achieved by a formation of plasma self-generated bootstrap currents (Bickerton *et al.*, 1971), resulting from a pressure gradient in the plasmas. In general, the formation of internal transport barriers (ITBs) can provide a strong pressure gradient in the plasma core. Consequently, a large bootstrap current can be achieved in ITB plasma (Connor *et al.*, 2004). Thus, it is interesting to investigate the relation between bootstrap current and formation of ITB in the ITER.

It is accepted that formation of large bootstrap current is one of the crucial issues for nuclear fusion reactors using the tokamak concept. If a large bootstrap current fraction can be achieved, the inductive plasma current can be partially reduced or completely removed. A non-inductive current by bootstrap current has been observed in a number of present-day experiments and theoretical studies. Many techniques are used in the experiments to drive steady-state plasmas with full non-inductive current drive (Budny *et al.*, 2008; Murakami *et al.*, 2010; Nagashima *et al.*, 1997; Oyama *et al.*,

* Corresponding author.
Email address: thawatchai@siit.tu.ac.th

2009). In the Japanese JT-60U tokamak for fusion plasma research and development (Nagashima *et al.*, 1997; Oyama *et al.*, 2009), the neutral beam injections (NBI) were used to provide a long period of central heating to up to 30 seconds for maintaining an ITB. A strong peaked pressure profile yielded a large bootstrap current fraction (more than 40%) (Oyama *et al.*, 2009). Nagashima *et al.* (1977) (Nagashima *et al.*, 1997) showed the steady state operation region, determined by the density limit and the full non-inductive current drive condition in the JT-60U, by using 60 MW NBI heating. used the ONETWO code with GLF23 transport model and NCLASS (Houlberg *et al.*, 1997) to predict the results for the ITER steady state for bootstrap current fraction to be greater than 50%. Honda *et al.* (2004) combined NCLASS with a current diffusive ballooning mode (CDBM) transport model into the TASK/TR code (Honda *et al.*, 2006) and showed that the bootstrap current plays a significant role in forming the ITB and has a possibility to achieve long-time operation. The simulations using CRONOS (Basiuk *et al.*, 2003), indicated that the duration of a hybrid pulse sustained by 20 MW of ICRF and 30 MW of NBI could be extended from 400 sec to 1,000 sec when adding 20 MW of LHCD, and were shown by Kessel *et al.* (2007).

In this work, the relationships between bootstrap current and ITB formation in ITER with standard type I ELMy *H*-mode and steady state designed parameters are investigated using BALDUR integrated predictive modeling code (Singer *et al.*, 1988). In each simulation, a NCLASS module is used to predict neoclassical transport, while Mixed Bohm/gyro-Bohm (Mixed B/gB) model (Tala *et al.*, 2005) is used for anomalous core transport. Mixed B/gB model is a semi-empirical anomalous core transport model, which can include the effect of ITBs by suppressing anomalous transport due to $\omega_{E\times B}$ flow shear and magnetic shear. It has been intensively tested against various scenarios of experiments from different tokamaks; such as JET (Onjun *et al.*, 2004; Onjun *et al.*, 2004; Parail, 2002; Parail *et al.*, 1999; Snyder *et al.*, 2005; Tala *et al.*, 2006; Tala *et al.*, 2005; Tala *et al.*, 2002), DIII-D (Hannum *et al.*, 2001), and TFTR (Onjun *et al.*, 2001). The flow shear is calculated from a formation of an electric field, which requires the information of pressure gradient, toroidal velocity, and poloidal velocity. In this work, poloidal velocity is obtained from NLCASS prediction. There are three different choices for toroidal velocity (a strong, medium and zero), which will have an impact on the calculation of shearing rate, and, consequently, ITB. The ETB is described in terms of a pedestal model since the region considered in these simulations is up to the top of the pedestal. In all simulations, NCLASS module is used to predict bootstrap current according that particular plasma conditions. Note, that the calculation of bootstrap current using NCLASS has been used in various codes, such as JETTO (Cennacchi *et al.*, 1988), TASK, ONETWO, ASTRA (Pereverzev *et al.*, 2002) and BALDUR. Moreover, the optimal region for Fusion Q and bootstrap current fraction is investigated by varying the plasma current and line average density. In addition, the effect of heating power, pedestal temperature, and impurity content is studied.

This paper is organized as follows: brief information of the BALDUR integrated predictive modeling code describes the anomalous core transport model, NCLASS and pedestal model. The predictions of ITER for standard *H*-mode and steady state scenario are presented and discussed in Section 3. The sensitivity study is found in Section 4 and the final section is the summary.

2. BALDUR integrated predictive modeling code

The BALDUR integrated predictive modeling code is used to compute the time evolution of plasma profiles including electron and ion temperatures, hydrogenic (hydrogen and its isotope), and impurity densities, safety factor, neutrals, and fast ions. These time-evolving profiles are computed in the BALDUR code by combining the effects of many physical processes self-consistently, including the effects of transport, plasma heating, particle influx, boundary conditions, the plasma equilibrium shape, and sawtooth oscillations. Fusion heating and helium ash accumulation are also computed self-consistently. BALDUR simulations have been intensively compared against a variety of plasma experimental data, which yield an overall agreement with about a 10% relative RMS deviation. In the BALDUR code, fusion heating power is determined by the nuclear reaction rates together with a Fokker Planck package used to compute the slowing down spectrum of fast alpha particles on each flux surface in the plasma. The fusion heating component of the BALDUR code also computes the rate of the production of thermal helium ions and the rate of the depletion of deuterium and tritium ions within the plasma core. For the ITER case, BALDUR code has been intensively used to simulate ITER plasma in the various aspects (Bateman *et al.*, 2003; Kinsey *et al.*, 2003; Mukhovatov *et al.*, 2003; Onjun, 2009, 2009; Onjun *et al.*, 2008).

2.1 Mixed B/gB anomalous transport model

Mixed B/gB model (Erba *et al.*, 1997) is a semi-empirical anomalous core transport model. It was originally a local transport model with Bohm scaling. A transport model is said to have "Bohm" scaling when the transport diffusivities are proportional to the gyro-radius times thermal velocity. Transport diffusivities in models with Bohm scaling are also functions of the profile shapes (characterized by normalized gradients) and other plasma parameters, such as magnetic q. These parameters are held fixed in systematic scans in which only the gyro-radius is changed relative to plasma dimensions. The original model was subsequently extended to describe ion transport, and a gyro-Bohm term was added in order to produce simulation results that match data from smaller tokamaks as well as data from larger machines. A transport model is said to have "gyro-Bohm" scaling when the transport diffusivities are proportional to the square of

the gyro-radius times thermal velocity divided by a plasma linear dimension, such as the major radius. The Bohm contribution to the original model usually dominates over most of the plasma. The gyro-Bohm contribution usually makes its largest contribution in the deep core of the plasma and plays a significant role only in smaller tokamaks with relatively low heating power and low magnetic field. To include the ITB effect, the Bohm contribution is modified by a cut-off that is a function of magnetic and flow shear. The Mixed Bohm/gyro-Bohm transport model with ITB effect included and ITB is formed by the suppression of core anomalous transport due to $\omega_{\mathbf{E\times B}}$ flow shear and magnetic shear. The Mixed Bohm/gyro-Bohm transport model with ITB effect included can be expressed as follows (Tala *et al.*, 2001):

$$\chi_e = 1.0\chi_{gB} + 2.0\chi_B \tag{1}$$

$$\chi_i = 0.5\chi_{gB} + 4.0\chi_B + \chi_{neo} \tag{2}$$

$$D_H = \left[0.3 + 0.7\rho\right]\frac{\chi_e\chi_i}{\chi_e + \chi_i} \tag{3}$$

$$D_Z = D_H \tag{4}$$

where

$$\chi_{gB} = 5\times10^{-6}\sqrt{T_e}\left|\frac{\nabla T_e}{B_\phi^2}\right| \tag{5}$$

$$\chi_B = 4\times10^{-5} R\left|\frac{\nabla\left(n_e T_e\right)}{n_e B_\phi}\right| q^2\left(\frac{T_{e,0.8} - T_{e,1.0}}{T_{e,1.0}}\right)$$

$$\Theta\left(-0.14 + s - \frac{1.47\omega_{E\times B}}{\gamma_{ITG}}\right) \tag{6}$$

In these expressions, the χ_e is the electron diffusivity, χ_i is the ion diffusivity, D_H is the particle diffusivity, D_z is the impurity diffusivity, χ_{gB} is the gyro-Bohm contribution, χ_B is the Bohm contribution, ρ is normalized minor radius, T_e is the local electron temperature in keV, B_ϕ is the toroidal magnetic field, R is the major radius, n_e is the local electron density, q is the safety factor, s is the magnetic shear $[r\,(\mathrm{d}\,q\,/\,\mathrm{d}r)\,/\,q]$, ω_{ExB} is the flow shearing rate, and the γ_{ITG} is the ITG growth rate, estimated as v_{ti}/qR, in which v_{ti} is the ion thermal velocity. The role of impurity transport is very complicated and crucial for burning plasma experiments since it controls impurity behavior, such as helium ash accumulation. Since the original Mixed B/gB model does not include impurity transport, in this work, it is assumed that the impurity transport is equal to the particle transport. In this work, the ω_{ExB} shearing rate is calculated as follows (Waltz *et al.*, 1997):

$$\omega_{ExB} = \left|\frac{RB_\theta^2}{B_\phi}\frac{\partial\left(E_r/RB_\theta\right)}{\partial\psi}\right|, \tag{7}$$

where R is the major radius, B_θ and B_ϕ are the poloidal and toroidal magnetic fields, respectively, Ψ is the poloidal flux, and E_r is the radial electric field for the main plasma ions, which is calculated using a force balance equation as follows:

$$E_r = \frac{1}{Zen_i}\frac{\partial p_i}{\partial r} - v_\theta B_\phi + v_\phi B_\theta, \tag{8}$$

where $\frac{\partial p_i}{\partial r}$ is the pressure gradient, v_θ and v_ϕ are the poloidal and toroidal velocities, respectively, and n_i is the ion density, Z is the ion charge number and e the elementary charge. As seen in Equation 7 and 8, the toroidal velocity is one of the terms used in the calculation of the radial electric field and the ω_{ExB} shearing rate. However, the exact calculation of toroidal velocity is complicated because it requires much information. Currently there is no a simple acceptable model to describe toroidal velocity. In fact, there was an attempt by Chatthong, (2010) to develop a simple toroidal velocity model (Chatthong *et al.*, 2010). However, it is not widely accepted due to the lack of crucial physical parameters such as plasma torque. Thus, in this work, the investigation was set up in the following way: three choices of toroidal velocity (strong, weak, and none) were used. For the strong and weak toroidal velocity cases, the toroidal velocity was taken directly from the JET experiment discharge 40542 and 40847, respectively. In addition, the variations of the toroidal velocity were examined to test the performance (Fusion Q and Current fraction) of H-mode and steady state scenarios.

2.2 NCLASS module

The NCLASS module calculates the neoclassical transport properties of multi-species axisymmetric plasma of arbitrary aspect ratio, geometry and collisionality. The neoclassical effects refer to the flows resulting from coulomb collisions between particles drifting in non-uniform magnetic and electric fields. This module determines a multi-fluid model for the parallel and radial force balance equations, giving the neoclassical bootstrap current, parallel electrical resistivity, impurity and fuel ion radial particle transport, ion radial thermal transport and plasma poloidal rotation (Houlberg *et al.*, 1997). It is designed to be called from a transport code that provides the plasma density, temperature profiles, and a number of flux surface averaged geometric quantities.

2.3 Pedestal model

In the expansion of the pedestal temperature models described in reference (Onjun et al., 2002), two ingredients are required: the pedestal width (Δ) and the pressure gradient ($\partial p/\partial r$). If the pedestal density (n_{ped}) is known, the temperature at the top of the pedestal (T_{ped}) can be estimated as

$$T_{ped} = \frac{1}{2n_{ped}k}\left|\frac{\partial p}{\partial r}\Delta\right| = \frac{\Delta}{2kn_{ped}}\frac{\alpha_c B_\phi^2}{2\mu_0 Rq^2}. \tag{9}$$

where k is the Boltzmann constant, μ_0 is the permeability of free space, α_c is the normalized critical pressure gradient,

In this work, one of the best pedestal temperature models in reference (Onjun *et al.*, 2002), is selected. This pedestal temperature model is based on the magnetic and flow shear stabilization width scaling ($\Delta\alpha\rho s^2$) (Sugihara *et al.*, 2000), where ρ is the ion gyro radius, and s is the magnetic shear. The pedestal pressure gradient calculation is normally complicated and requires a number of details. For simplicity, the pedestal gradient is assumed to be uniform throughout the pedestal region and the pedestal gradient is limited by the first stability limit of infinite n ballooning mode, so that the normalized critical pressure gradient for the pedestal region is estimated by

$$\alpha_c \equiv -\frac{2\mu_0 R q^2}{B_\phi^2}\left(\frac{\partial p}{\partial r}\right)_c = 0.4s\left(1+\kappa_{95}^2(1+5\delta_{95}^2)\right). \quad (10)$$

The pedestal density is described by a simple empirical model. Since the pedestal density n_{ped}, is usually a large fraction of line average density, n_l, the pedestal density can be calculated as:

$$n_{ped} = 0.71 n_l \quad (11)$$

This pedestal density model agrees with the pedestal data obtained from the ITPA pedestal database with 12% RMSE (Sugihara *et al.*, 2003). In this work, it is assumed that the impurity consists of helium and beryllium. The ratio of helium to electron density at the edge is 1%. The effective charge is about 1.4 at the edge of the plasma. With these conditions of the impurity, the densities of beryllium and helium at the boundary are $1.3\text{x}10^{18}$ m^{-3} and $1.0\text{x}10^{18}$ m^{-3}, respectively.

3. Simulation results and Discussion

The BALDUR code was used to carry out simulations of ITER with the design parameters for full-current standard type I ELMy *H*-mode discharge ($R = 6.2$ m, $a = 2.0$ m, $I_p = 15$ MA, $B_\phi = 5.3$ T, $\kappa_{95} = 1.7$, $\delta_{95} = 0.33$, $n_l = 1.0\text{x}10^{20}$ m^{-3} and $Z_{eff} = 1.4$) and steady state *H*-mode discharge ($R = 6.2$ m, $a = 2.0$ m, $I_p = 9$ MA, $B_\phi = 5.3$ T, $\kappa_{95} = 2.0$, $\delta_{95} = 0.5$, $n_l = 0.7\text{x}10^{20}$ m^{-3} and $Z_{eff} = 1.4$). In all simulations, the plasma current and density were slowly ramped up to the target values within the first 100 sec of the simulation with the target plasma current at 15 MA in *H*-mode scenario and 9 MA in steady state scenario, as shown in Figure 1.

In the case of standard *H*-mode, the total auxiliary heating power used in the simulation was 40 MW, which consists of two different sources. The first 33 MW came from NBI heating power, and 7 MW came from RF heating. The RF heating power was increased to 20 MW to generate total plasma current in long pulsed operation. It is worth noting that there were several physical processes that have not been included in these simulations, such as ELM crashes and neoclassical tearing modes. Consequently, the simulation results did not represent the complete dynamic behaviors of the ITER plasma. However, it was expected that these simulations included sufficient physics to describe the plasma when it reached a quasi-steady state with sawtooth oscillations. The simulations yield complex and interesting interactions within the plasma itself such as the self heating of the plasma by the production of fast alpha particles and redistribution of heating power after each sawtooth crash. Sawtooth oscillations

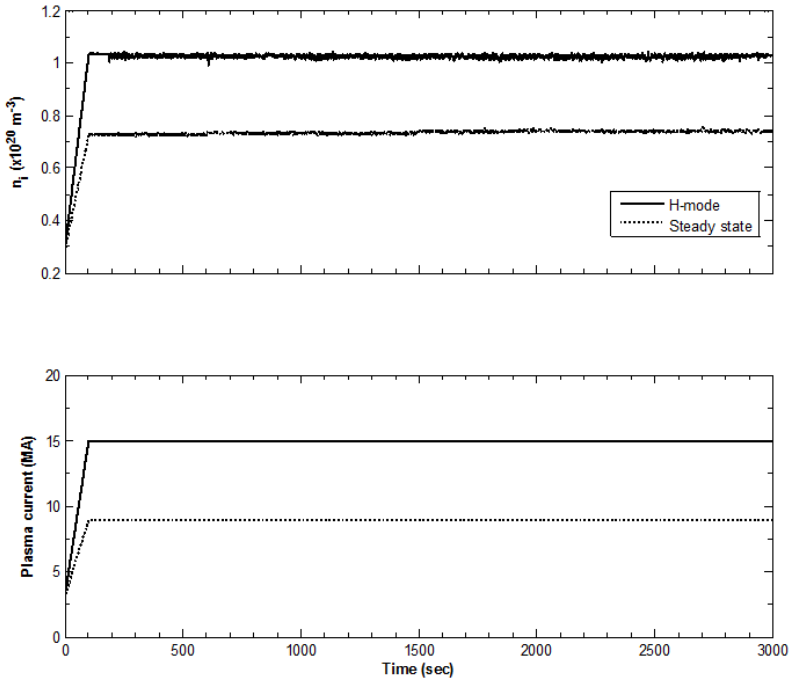

Figure 1. Time evolution of line average density (top) and plasma current (bottom).

were considered during these simulations. The Porcelli sawtooth model (Porcelli *et al.*, 1996) was used to trigger sawtooth crashes and a modified Kadomtsev magnetic reconnection model (Bateman *et al.*, 2006) was used to compute the effects of each sawtooth crash. Note, that during each sawtooth crash, it is assumed that 10% of magnetic flux was mixed to describe the effect of each sawtooth crash. For each simulation, anomalous transport was calculated using the Mixed B/gB transport model with the effect of ITB included, while the bootstrap current and neoclassical transport were predicted using the NCLASS module. It is worth noting that plasma profiles, including the bootstrap current, were simulated from the center of plasma to the top of edge transport barrier due to a limitation of grid-resolution in BALDUR code. As a result, the bootstrap current in the edge region was not included. Since the bootstrap current could be significant in the edge region due to a large pressure gradient and volume in the edge region, the results obtained for bootstrap current fraction could be treated as the minimum.

During the slow current ramp up phase (reaching the target value in 100 sec), the plasma density was also ramped up to the target plasma density at the same time with the plasma current with full auxiliary heating power applied starting from the beginning of the simulations. In this work, the $\omega_{\mathbf{E\times B}}$ shearing rate profile for initiating a formation of an ITB was calculated using Equation 7, while the toroidal velocity is either taken to be zero or taken directly from the Joint European Torus (JET) experiments: either discharge 40542 for strong toroidal velocity case or discharge 40847 for medium toroidal velocity case. In Figure 2, the self-consistently predicted $\omega_{\mathbf{E\times B}}$ profiles at a time before sawtooth crash using Equation 7 were shown for standard *H*-mode and steady state scenarios. When the toroidal velocity from JET discharge 40542 was used, it could be seen that the peak value of calculated $\omega_{\mathbf{E\times B}}$ shearing rate for ITER was located at the radial position =0.53 with slightly different values: -2.55x10^5 s^{-1} for standard *H*-mode and -2.25x10^5 s^{-1} for steady state. However, when the toroidal velocity from JET discharge 40847 was used, the minimum value of $\omega_{\mathbf{E\times B}}$ was also located at the same position ρ =0.40 with also slightly different values: -1.80x10^5 s^{-1} for standard *H*-mode scenario and -1.40x10^5 s^{-1} for steady state scenario. Finally, for the zero toroidal velocity case, it could be seen that the value of calculated $\omega_{\mathbf{E\times B}}$ shearing rate was close to zero for both ITER scenarios, which implies that the ITB formation in this case results only from the magnetic shear effect. Note that both flow shear and magnetic shear could result in the formation of ITB in the Mixed B/gB transport model.

Figure 3, 4, and 5 show the plasma profiles of *H*-mode and steady state with and without ITB for ion temperature, ion density, ion thermal transport coefficient, hydrogenic transport coefficient, total current density, and bootstrap current density as a function of normalized minor radius at a time before a sawtooth crash. Note, that the electric field for $E_r \times B$ flow shear calculation was predicted using the toroidal velocity either from JET discharge 40542 (strong v_ϕ) or from JET discharge 40847 (medium v_ϕ) or using a zero toroidal velocity. The pedestal temperature model based on magnetic and flow shear stabilization was used for these simulations. The simulations were carried out using the Mixed B/gB transport model with the effects of ITB included and excluded. In general, many theoretical models for ITB formation relied on the suppression of micro–instability, in which the ion thermal transport coefficient changes abruptly at the ITB foot (Connor *et al.*, 2004). This induces transport by sheared $E_r \times B$ flows (Oyama *et al.*, 2009) which were related to the toroidal

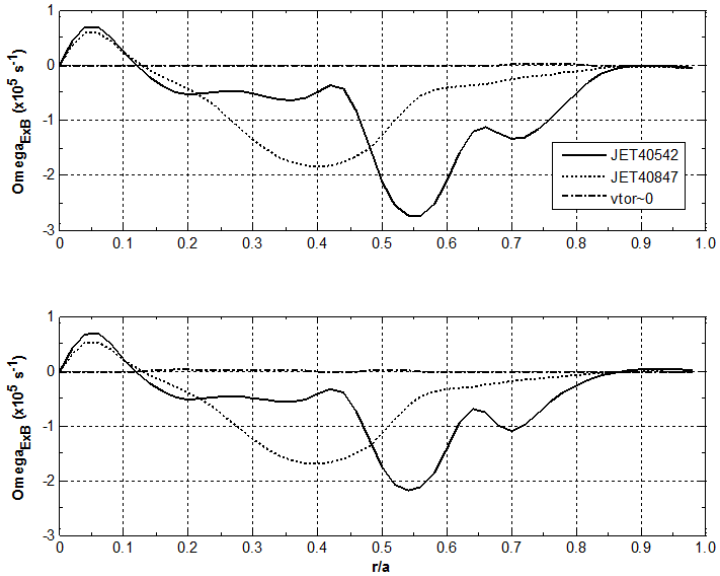

Figure 2. $\omega_{E\times B}$ profile plotted as a function of a normalized minor radius. Toroidal velocity is taken from JET experiment discharge 40542, 40847 and v_{tor}~0, while the $\omega_{E\times B}$ is calculated at a time before the sawtooth crash at 2,900 sec. The top panel is the *H*-mode scenario and the bottom panel is steady state scenario.

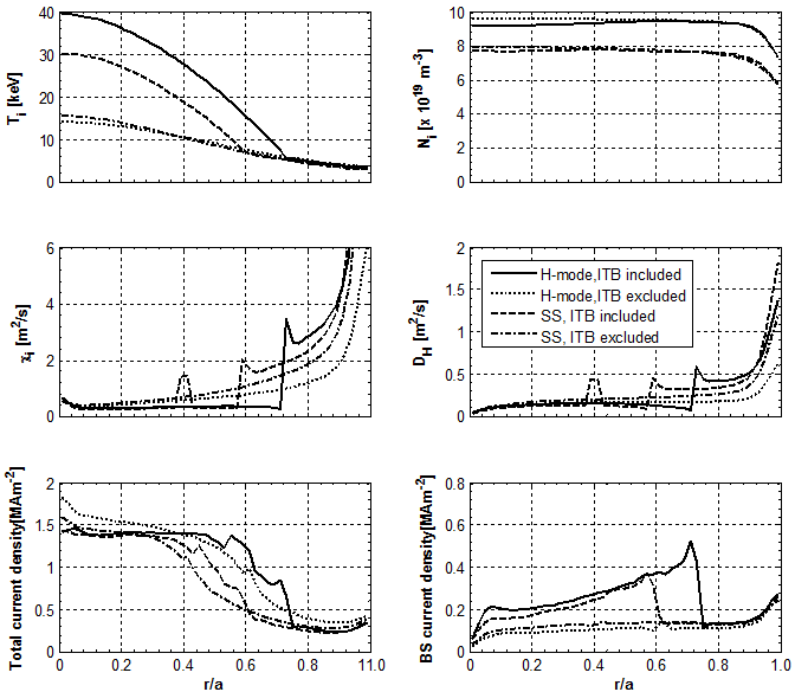

Figure. 3: Profile of *H*-mode and Steady State (SS) for ion temperature, ion density, ion thermal diffusivity, hydrogenic diffusivity, total current density and bootstrap current density are plotted as a function of a normalized minor radius at a time before a sawtooth crash. The electric field for $E_r \times B$ flow shear estimation is calculated using the toroidal velocity from the JET experiment (JET 40542). The simulations are carried out with and without ITB effects. The boundary condition is provided by the pedestal model, based on magnetic and flow shear stabilization.

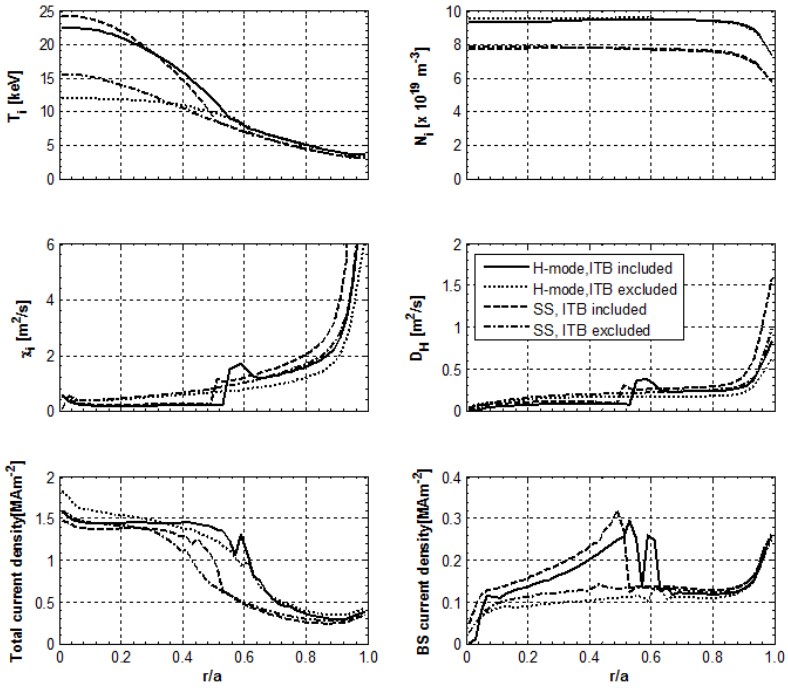

Figure 4. Profile of *H*-mode and Steady State (SS) for ion temperature, ion density, ion thermal diffusivity, hydrogenic diffusivity, total current density and bootstrap current density are plotted as a function of a normalized minor radius at a time before a sawtooth crash. The electric field for $E_r \times B$ flow shear estimation is calculated using the toroidal velocity from the JET experiment (JET 40847). The simulations are carried out with and without ITB effects. The boundary condition is provided by the pedestal model, based on magnetic and flow shear stabilization.

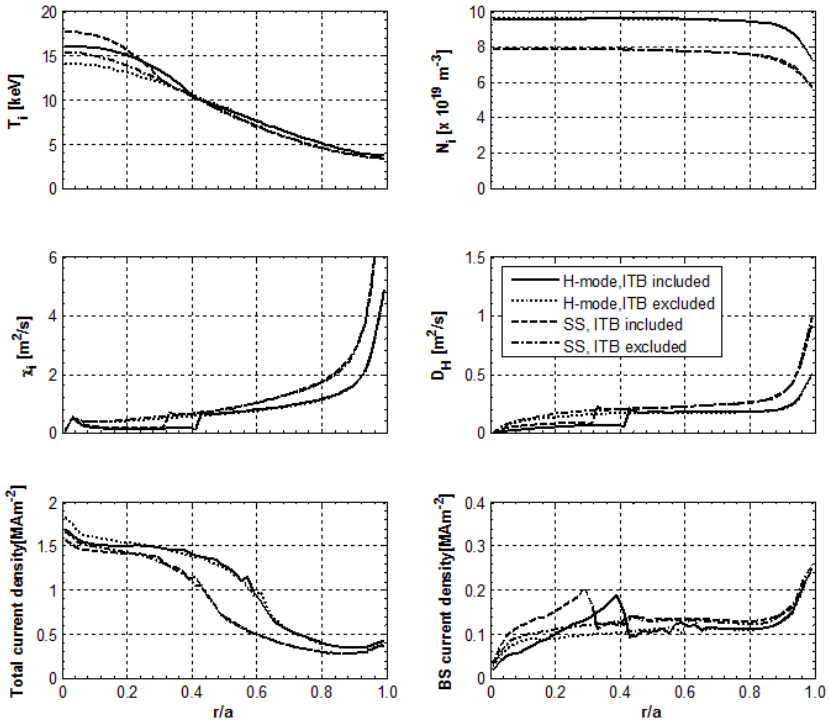

Figure 5. Profile of *H*-mode and Steady State (SS) for ion temperature, ion density, ion thermal diffusivity, hydrogenic diffusivity, total current density and bootstrap current density are plotted as a function of a normalized minor radius at a time before a sawtooth crash. The electric field for $E_r \times B$ flow shear estimation is calculated using the toroidal velocity to be zero. The simulations are carried out with and without ITB effects. The boundary condition is provided by the pedestal model, based on magnetic and flow shear stabilization.

velocity. It could be seen in Figure 3 and 4 that, when the ITB effects were included in the simulation, the ion central temperature increases significantly, depending on the magnitude of $\omega_{\mathbf{E\times B}}$ flow shear, while the temperatures near the plasma edge change just slightly among these simulations. In Figure 5, the simulation was carried out using a zero toroidal velocity. The formation of ITB is established near the plasma core at $\rho = 0.4$ for *H*-mode and $\rho = 0.3$ for steady state. It could be seen that ITER ion central temperature in the case of zero toroidal velocity was noticeably lower than those in the strong (40542) and medium (40847) $\omega_{\mathbf{E\times B}}$ cases. It was found in all simulations that the ion pedestal temperatures remain almost constant after the plasma density reaches its target value. Note, that the ion pedestal temperature was assumed to be the same as the electron pedestal temperature in this model. For the ion density, the core profile was nearly flat and separate into the density target of *H*-mode and steady state with relatively limited central peaking. The ion (χ_i) thermal transport and hydrogenic (D_H) transport coefficients as functions of normalized minor radius show the reduction of transport in the region close to the plasma core. The transport coefficient profiles when ITB was included were lower than that without ITB because the formation of ITB results in a reduction of the core transport for both energy and particles. The region of core transport reduction was associated with the ITB affected region. The bootstrap current density increases from the plasma center to the location of the ITB bottom and then decreases quickly toward the plasma edge. In Figure 3, the maximum bootstrap current density in the simulation using the toroidal velocity from JET discharge 40542 for predicting $\omega_{\mathbf{E\times B}}$ was located at $\rho = 0.75$ with the magnitude of 0.50 MA/m^2 for the standard *H*-mode scenario and at $\rho = 0.58$ with the magnitude of 0.38 MA/m^2 for steady-state scenario. In Figure 4, the maximum bootstrap current density in the simulation using the toroidal velocity from JET discharge 40847 for predicting $\omega_{\mathbf{E\times B}}$ was located at $\rho = 0.52$ with the magnitude of 0.30 MA/m^2 for the standard *H*-mode scenario and at $\rho = 0.48$ with the magnitude of 0.31 MA/m^2 for steady-state scenario. In Figure 5, the maximum bootstrap current density in the simulation using zero toroidal velocity for predicting $\omega_{\mathbf{E\times B}}$ is located at $\rho =$ 0.40 with the magnitude of 0.20 MA/m^2 for the standard *H*-mode scenario and at $\rho = 0.18$ with the magnitude of 0.20 MA/m^2 for steady-state scenario. It is worth pointing out that the location of maximum bootstrap current density was associated with the location of the ITB bottom. It should be noted that due to the limit of grid points in BALDUR code, in this work the simulations were carried out from the centre of the plasma to the top of barrier. As a result, the bootstrap current in the pedestal region did not include, which could be significant because of the ETB and large volume at the edge. Therefore, it was better to treat the results obtained in this

Table 1. Notation used in this paper

Symbol	Unit	Description
R	m	Major radius
a	m	Minor radius
I_p	MA	Plasma current
B_ϕ	Tesla	Toroidal magnetic field
B_θ	Tesla	Poloidal magnetic field
κ_{95}	-	Elongation at 95% of
δ_{95}	-	Triangularity at 95% of
n_e	m^{-3}	Electron density
n_l	m^{-3}	Line average density
q	-	Safety factor
s	-	Magnetic shear
$\omega_{B\times E}$	s^{-1}	Flow shearing rate
χ_i	m^2/s	Ion thermal diffusivity
χ_e	m^2/s	Electron thermal diffusivity
D_H	m^2/s	Hydrogenic particle diffusivity
D_z	m^2/s	Impurity particle diffusivity
χ_B	m^2/s	Bohm contribution
χ_{gB}	m^2/s	gyro-Bohm contribution
χ_{neo}	m^2/s	Neoclassical contribution
v_{ti}	m/s	Thermal velocity
γ_{ITG}	s^{-1}	ITG growth rate
ρ_i	m	Ion gyro radius
ρ	-	Normalized minor radius
T_e	keV	Electron temperature
T_i	keV	Ion temperature
T_{ped}	kev	Pedestal temperature
n_{ped}	m^{-3}	Pedestal density
α_c	-	Normalized pressure gradient
Z_{eff}	-	Effective charge

work as the minimum value. In Figure 3, 4, and 5, the alpha power of *H*-mode was higher than the steady state scenario in every case, which implies that the Fusion *Q* of *H*-mode to be much higher than the Fusion *Q* of steady state scenario, too.

In both standard *H*-mode and steady state scenario, the average of alpha power during the period from 2,900 to 3,000 sec was summarized in Table 2, 3, and 4. The fusion performance could be evaluated in terms of the Fusion *Q*, which could be calculated as:

$$\text{Fusion } Q = \frac{5 \times P_{\alpha,\text{avg}}}{P_{\text{aux}}} \tag{12}$$

where $P_{\alpha,\text{avg}}$ is a time-average of the alpha power and P_{aux} is the auxiliary heating power (equal to 40 MW for standard *H*-mode scenario and 53 MW for steady state scenario). Note, that these results were obtained from the simulations using the pedestal model based on the magnetic and flow shear stabilization concept together with the infinite-*n* ballooning stability concept. It was shown in Onjun *et al.* (2001) that the simulations using the pedestal models developed in (Snyder *et al.*, 2005), which relied on an estimation of the first stability regime of ballooning modes, yielded similar predictions. It could be seen in Table 2, when using the toroidal velocity from JET 40542 that Fusion *Q* improved to 17.97 and bootstrap current fraction (f_{bs}) increased to 0.35. While in the steady state, the Fusion *Q* is 4.35 and f_{bs} was 0.36. In this scenario, Fusion *Q* was slightly lower than the target of Fusion *Q* and was greater or equal to 5.00, but f_{bs} is much lower than the target.

4. Sensitivity Study

In this section, the parametric sensitivity of BALDUR simulation was investigated by varying some plasma parameters: plasma current, line average density, heating power, pedestal temperature, and impurity content. Since the trend of both standard *H*-mode and steady state were similar, the work was focused on only the steady state scenario. The effects of varying the plasma current and the line average density were studied and discussed in Section 4.1. In Section 4.2, the effects of varying heating power that produce the total bootstrap current were investigated. The effects of varying pedestal temperature and effective charge were studied in Section 4.3 and 4.4, respectively. It should be noted that in these sections, a fixed pedestal temperature at 4.0 keV was used, except in the Section 4.3, in which the pedestal value was varied.

Table 2. Summary of average alpha power, Fusion *Q* during the last 50 sec of the simulations from 2,900 sec to 3,000 sec and Bootstrap current fraction (<J_boot>/<J_tor>) at time 2,990 sec, when the pedestal model is based on magnetic flow shear stabilization ($\Delta\alpha\rho s^2$), and the electric field for $E_r \times B$ flow shear estimation is calculated using the toroidal velocity from the JET experiment (JET 40542).

Parameters	Standard *H*-mode			Steady State		
	w/o ITB	with ITB	% change	w/o ITB	with ITB	% change
$P_{\alpha,\text{avg}}$ [MW]	20	144	620	3.3	46	1294
Fusion Q_{avg}	2.5	18.0	620	0.3	4.3	1333
BS Current Fraction	0.12	0.35	192	0.16	0.36	125

Table 3. Summary of average alpha power, Fusion Q during the last 50 sec of the simulations from 2,900 sec to 3,000 sec and Bootstrap current fraction (<J_boot>/<J_tor>) at time 2,990 sec, when the pedestal model is based on magnetic flow shear stabilization ($\Delta\alpha\rho s^2$), and the electric field for $E_r \times B$ flow shear estimation is calculated using the toroidal velocity from the JET experiment (JET 40847).

Parameters	Standard H-mode			Steady State		
	w/o ITB	with ITB	% change	w/o ITB	with ITB	% change
$P_{\alpha,avg}$ [MW]	20	41	105	3	16	433
Fusion Q_{avg}	2.5	5.1	104	0.3	1.5	400
BS Current Fraction	0.12	0.20	67	0.16	0.21	31

Table 4. Summary of average alpha power, Fusion Q during the last 50 sec of the simulations from 2,900 sec to 3,000 sec and Bootstrap current fraction (<J_boot>/<J_tor>) at time 2,990 sec, when the pedestal model is based on magnetic flow shear stabilization ($\Delta\alpha\rho s^2$), and the electric field for $E_r \times B$ flow shear estimation is calculated using zero toroidal velocity.

Parameters	Standard H-mode			Steady State		
	w/o ITB	with ITB	% change	w/o ITB	with ITB	% change
$P_{\alpha,avg}$ [MW]	20	13	-35	3	3	0
Fusion Q_{avg}	2.5	1.6	-36	0.3	0.3	0
BS Current Fraction	0.12	0.14	17	0.16	0.16	0

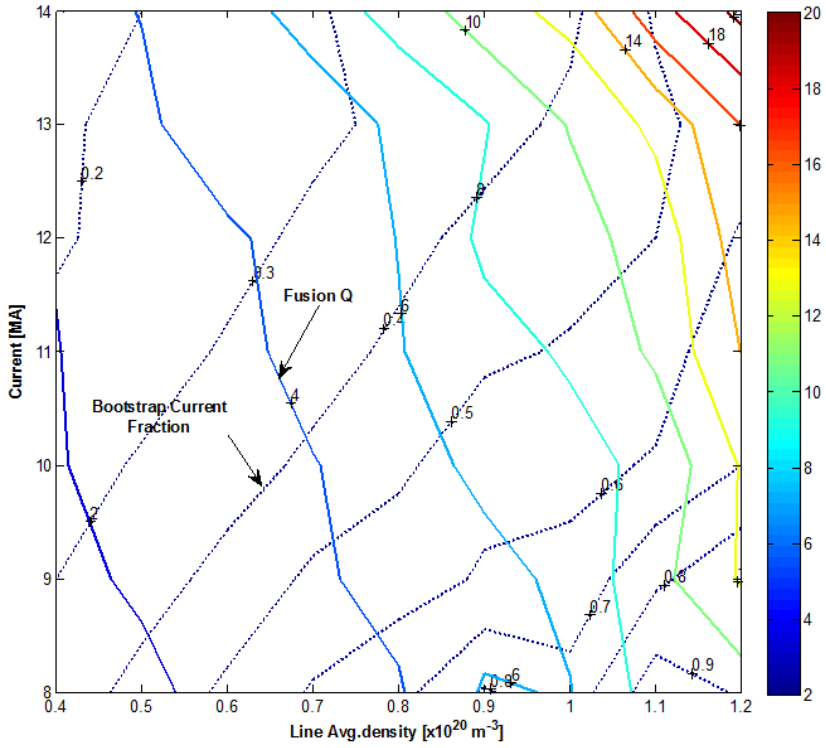

Figure 6. Optimal region for steady state scenario as a contour plot of bootstrap current fraction and Fusion Q as a function of plasma current and line average density, when using toroidal velocity for JET 40542 discharge.

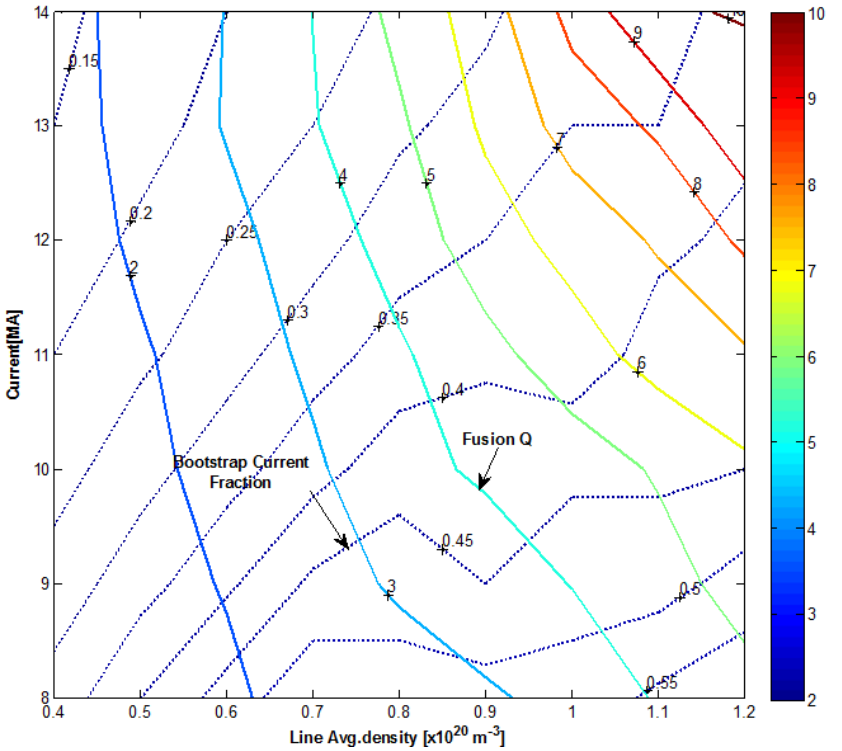

Figure 7. Optimal region for steady state scenario as a contour plot of bootstrap current fraction and Fusion Q as a function of plasma current and line average density, when using toroidal velocity for JET 40,847 discharge.

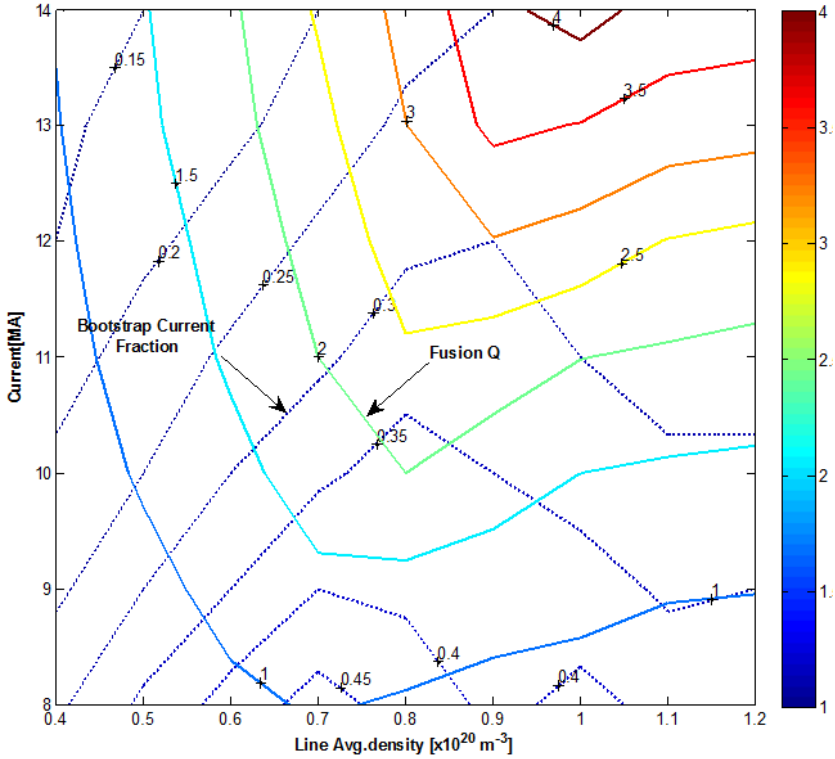

Figure 8. Optimal region for steady state scenario as a contour plot of bootstrap current fraction and Fusion Q as a function of plasma current and line average density, when using toroidal velocity to be zero (v_{tor}~0).

4.1 Variation of plasma current and line average density

It is well known that increasing of plasma current results in better plasma confinement, which can improve the plasma performance and the formation of bootstrap current. However, costs of construction and operation will increase. The issue of plasma current must be carefully evaluated. In addition, increasing the plasma density can yield better fusion performance. As a result, the operating density in burning plasma experiments is designed to be as high as possible. In the experiment, the operation can be limited by the density limit (normally represented in term of Greenwald density) and instabilities, which can result in a major disruption. It was found in JT-60 that stable operation above the Greenwald limit is possible if high Z metals are used for divertor (Nagashima *et al.*, 1997).

In this work, the impact of plasma current and line average density variation was investigated and the results were shown in Figure 6, 7, and 8. These figures show the bootstrap current fraction (f_{bs}) and Fusion Q for the simulations using the strong (JET 50,542), medium (JET 40847), and zero toroidal velocity, respectively. The f_{bs} and Fusion Q were projected on the current and density plane to predict the optimal region between bootstrap current and plasma performance. In the strong toroidal velocity case, showing in Figure 6, the solid line represents constant Fusion Q and the dash line represents constant f_{bs} . In the case of fixing Fusion Q, the line which represents Fusion Q is equal to 6.0. Moving up along this line, f_{bs} decreased while the plasma current increased and the line average density decreased. When moving down along this line, f_{bs} increased while the plasma current decreased but line, and the average density increased. When f_{bs} was fixed, the line which represents f_{bs} was equal to 0.5. Moving up along this line, Fusion Q increased while the plasma current increased and line average density increased. Moving down along this line, the Fusion Q decreased while the plasma current decreased and the line average density decreased. Figure 7 and 8 show the same trend but the f_{bs} and Fusion Q were reduced by the lower toroidal velocity. If one targets the bootstrap current of 0.5 and Fusion Q of 5, it required a plasma current of 10 MA and density of 0.8×10^{20} m^{-3} for a strong toroidal velocity of the plasma current of 9 MA and density of 1.15×10^{20} m^{-3} for medium toroidal velocity. For zero toroidal velocity, this case was out of range.

4.2 Bootstrap current driven by NBI

There were many techniques used to drive the bootstrap current in steady state operation. One very efficient technique was Neutral Beam Injection (NBI) because it did not depend on any resonance conditions or coupling conditions at the edge. NBI heating was used and its impact was investigated by varying the power (23, 33, and 43 MW). Note, that the NBI heating of 33 MW was the designed parameter. In Figure 9, the pedestal temperature model was based on the magnetic and flow shear stabilization and the toroidal velocity from JET 40542 was used in this simulation. The

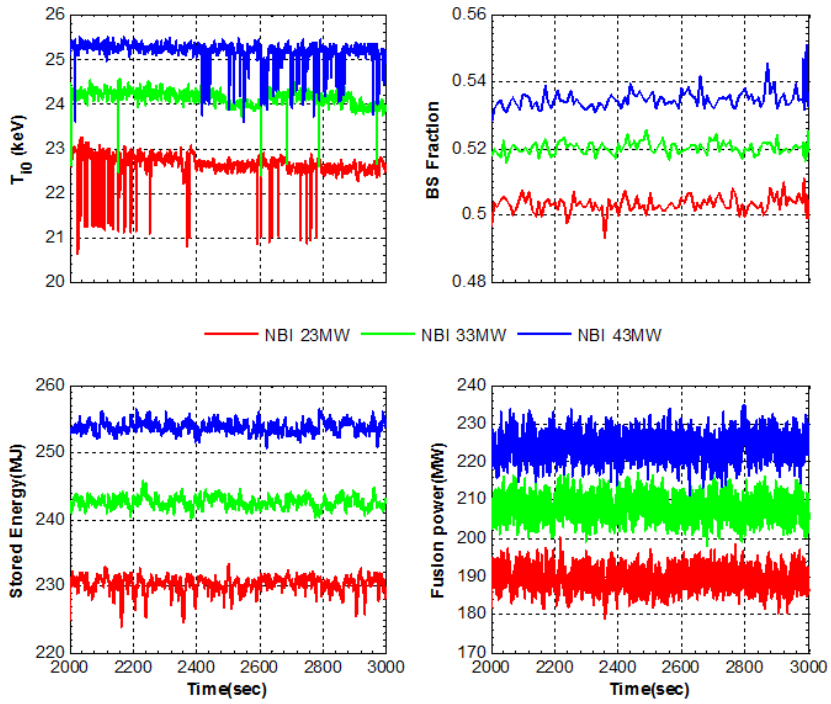

Figure 9. Steady state scenario of central ion temperature, bootstrap current fraction, total stored energy and fusion power as a function of time (2,000-3,000 sec). The simulations are carried out with ITB effects and NBI power is 23, 33, and 43 MW. Boundary condition is provided by the fixed pedestal temperature model.

percentages of bootstrap current, when NBI power was varied, were 34.9, 37.3, and 37.3, respectively. However, the variation of NBI power did not effect the location of ITB and the profile of $\omega_{\mathbf{E\times B}}$. It should be noted that the total bootstrap current in this work was calculated from the center of the plasma to the top of the barrier which was most of the

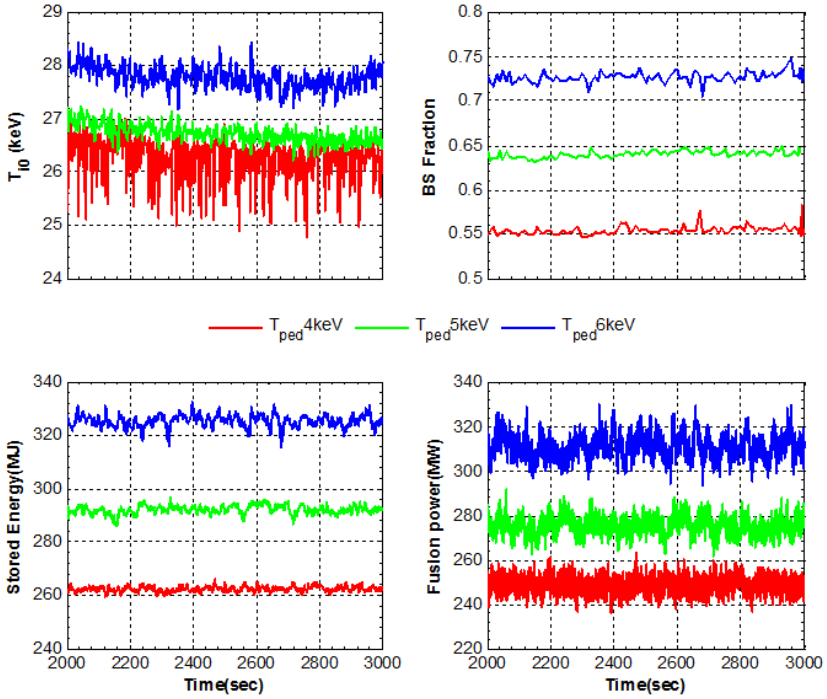

Figure 10. Steady state scenario of central ion temperature, bootstrap current fraction, total stored energy and fusion power as a function of time (2,000-3,000 sec). The simulations are carried out with ITB effects and pedestal temperature (T_{ped}) is 4, 5, and 6 keV. Boundary condition is provided by the fixed pedestal temperature model.

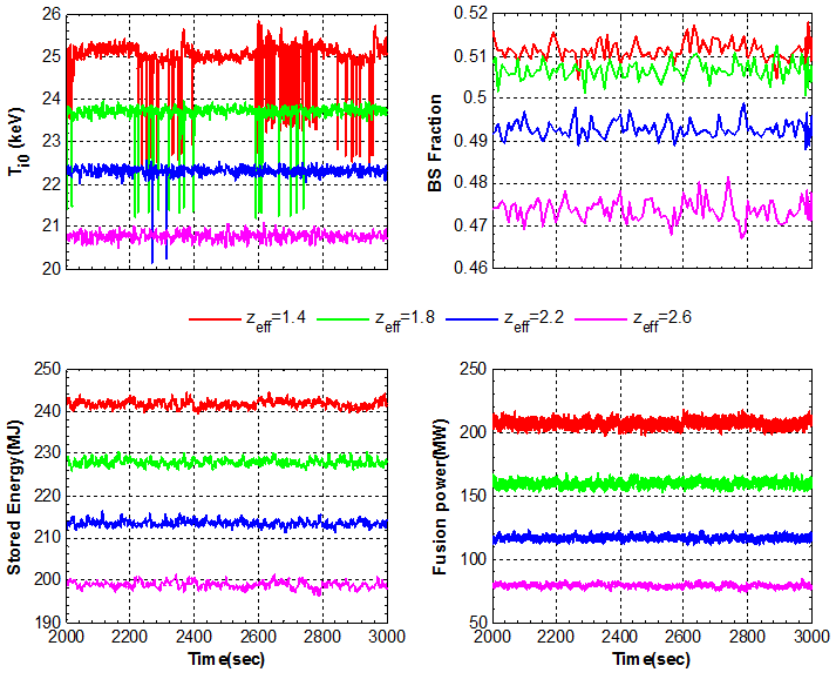

Figure 11. Steady state scenario of central ion temperature, bootstrap current fraction, total stored energy and fusion power as a function of time (2,000-3000 sec). The simulations are carried out with ITB effects and edge effective charge ($Z_{eff,edge}$) is 1.4, 1.8, 2.2 and 2.6. Boundary condition is provided by the fixed pedestal temperature model.

plasma area. It did not include the bootstrap current at the edge of the plasma. The NBI power did not change significantly by ion and electron temperature. The ion and electron temperature remained constant after the plasma density reached its target value. The alpha power increased when the NBI power added more to the plasma.

4.3 Pedestal temperature

The tokamak plasmas will be greatly enhanced if they can access a better confinement operational regime known as *H*-mode. The key success of *H*-mode is formation of a transport barrier near the plasma edge, called the pedestal. The plasma performance in *H*-mode is strongly dependent on the temperature at the top of the pedestal due to stiffness of profiles. In this work, a fixed pedestal temperature was varied from 3, 4, and 5 keV. Note, that the predicted pedestal temperature using the model in the previous section, was close to 3 keV, which yield quite pessimistic results. The results were shown in Figure 10, which was the time evolution of central temperature, bootstrap current fraction, total stored energy and total alpha power. It could be seen that, increasing the pedestal temperature, increases all parameters, but any changes of the pedestal temperature did not affect the location of ITB and the profile of $\omega_{\mathbf{E\times B}}$. The bootstrap current fraction increased when T_{ped} was increased, from 0.50, 0.64, and 0.73 for T_{ped} equaling to 4, 5, and 6 keV, respectively.

4.4 Effect of varying $Z_{eff,edge}$

It is well known that the impurity contamination largely influences the performance of magnetically confined plasmas in tokamak devices. The adoption of low Z materials, such as carbon (C), boron (B) and beryllium (Be), has led to large successes in present day experiments. Recently, the use of high Z materials such as molybdenum (Mo) and tungsten (W) is under continuous discussion, due to their low erosion rates and good thermal conductivity (Ohya *et al.*, 1999). For example, the JT-60U team used molybdenum coated with titanium carbide on divertor material. The effective charge number was less than two. However, the applicability of high Z materials is restricted by their high radiation losses, so the investigation of the different Z materials is emphasized in this section. In BALDUR, it is necessary to specify the boundary density for all species. Here, the values for deuterium, tritium and helium are specified, whereas beryllium boundary density is calculated from the edge effective charge $Z_{eff,edge}$. The standard value of $Z_{eff,edge}$ used in Section 3 was 1.4. Hence, in this section, the effect of increasing $Z_{eff,edge}$ was to simulate scenarios when there was a larger amount of impurity in the near-wall region. In this study, the values of $Z_{eff,edge}$ used in simulations are 1.4, 1.8, 2.2, and 2.6. All results in Figure 9 were composed of central ion temperature, bootstrap current fraction, total stored energy and total alpha power as a function of time. It could be seen that, a $Z_{eff,edge}$ of 1.4 gives the largest core T_i, total stored energy and total alpha power followed by $Z_{eff,edge}$ of 1.8, 2.2, and 2.6. This result could be explained by considering the radiation power loss. It is known that the radiation loss is directly proportional to the effective charge squared, which means higher an effective charge results in larger radiation loss and, consequently, lower temperature. For the bootstrap current fraction, the results showed the same trend as other parameters. The largest bootstrap current fraction was 0.51 (fusion power = 210 MW) at 1.4 of the effective charge and the lowest was 0.47 (fusion power = 80 MW) at 2.6 of the effective charge.

5. Conclusions

Self-consistent simulations of ITER have been carried out using the 1.5D BALDUR integrated predictive modeling code. The combination of an empirical transport model Mixed B/gB together with the pedestal models, which were based on magnetic flow shear stabilization pedestal width concept and ballooning mode limit pressure gradient scaling, was used to simulate the time evolution of plasma current, bootstrap current, temperature and density profile for ITER standard *H*-mode and steady state scenarios. It was found that the presence of ITB yields a significant improvement in the magnitude of bootstrap current fraction, depending on the toroidal velocity. The sensitivity study of bootstrap current fraction on some plasma parameters, including plasma current, line average density, heating power, pedestal temperature and impurity content, are also carried out to search for an optimal operational regime. When the plasma current and line average density were varied, a complex scenario is obtained. It was also found that the bootstrap current fraction could slightly increase with either increasing of NBI power or pedestal temperature. The impact of impurity accumulation was also investigated. It was found that higher impurity concentration results in a significant degradation of fusion performance, but smaller degradation for bootstrap current.

Acknowledgments

This work was supported by the Thailand Center of Excellence in Physics and the National Research University Project of Thailand Office of Higher Education Commission. Mr. Y. Pianroj thanks the Strategic Scholarships for Frontier Research Network for Thai Ph.D. Program.

References

Basiuk, V., Artaud, J. F., Imbeaux, F., Litaudon, C. X. and Becoulet, A. 2003. Simulations of steady-state scenarios for Tore Supra using the CRONOS code. Nuclear Fusion. 43, 822.

Bateman, G., Bandres, M., Onjun, T., Kritz, A. and Pankin, A. 2003. Integrated predictive modeling of high-mode tokamak plasmas using a combination of core and

pedestal models. Physics of Plasmas. 10, 4358.

Bateman, G., Nguyen, C. N., Kritz, A. H. and porcelli, F. 2006. Testing a model for triggering sawtooth oscillations in tokamaks. Physics of Plasmas. 13, 072505.

Bickerton, R. J., Connor, J. W. and Taylor, J. B. 1971. Diffusion Driven Plasma Currents and Bootstrap Tokamak. Nature Physical Science. 229, 110-112.

Budny, R. V., Andre, R., Bateman, G. et al. 2008. Predictions of H-mode performance in ITER. Nuclear Fusion. 48, 075005.

Cennacchi, G. and Taroni, A. 1988. JETTO: A free-boundary plasma transport code. JET Report JET-IR. 88.

Chatthong, B., Onjun, T. and Singhsomroje, W. 2010. Model for toroidal velocity in H-mode plasmas in the presence of internal transport barriers. Nuclear Fusion. 50, 064009.

Connor, J. W., Fukuda, T., Garbet, X. and Gormezano, C. 2004. A review of internal transport barrier physics for steady-state operation of tokamaks. Nuclear Fusion. 44, R1-R49.

Erba, M., Cherubini, A. and Parail, V. V. 1997. Development of a non-local model for tokamak heat transport in L-mode, H-mode and transient regimes. Plasma Physics and Controlled Fusion. 39, 261.

Hannum, D., Bateman, G. and Kinsey, J. 2001. Comparison of high-mode predictive simulations using Mixed Bohm/gyro-Bohm and Multi-Mode MMM95 transport models. Physics of Plasmas. 8, 964.

Honda, M. and Fukuyama, A. 2006. Comparison of turbulent transport models of L- and H-mode plasmas. Nuclear Fusion. 46, 580-593.

Honda, M., Fukuyama, A. and Yagi, M. 2004. Trasnsport simulation of internal transport barrier formation using various neoclassical transport models. Journal of Plasma Fusion Research SERIES. 6, 160-163.

Houlberg, W. A., Shaing, K. C., Hirshman, S. P. and Zarnstorff, M. C. 1997. Bootstrap current and neoclassical transport in tokamaks of arbitrary collisionality and aspect ratio. Physics of Plasmas. 4, 3230.

Kaname, I. 2010. ITER on the road to fusion energy. Nuclear Fusion. 50, 014002.

Kessel, C. E., Giruzzi, G., Sips, A. C. C. and Budny, R. V. 2007. Simulation of the hybrid and steady state advanced operating modes in ITER. Nuclear Fusion. 47, 1274-1284.

Kinsey, J., Bateman, G., Onjun, T. and Pankin, A. 2003. Burning plasma projections using drift-wave transport models and scalings for the H-mode pedestal. Nuclear Fusion. 43, 1845.

Mukhovatov, V., Shimonura, V., Polevoi, Y. and Shimada, M. 2003. Comparison of ITER performance predicted by semi-empirical and theory-based transport models Nuclear Fusion. 2003, 942.

Murakami, M., Giruzzi, G., Bonoli, P., Budny, R. V. and Fukuyama, A. 2010. Integrated Modeling of Steady-State Scenarios and Heating and Current Drive Mixes for ITER. Proceedings of the 23rd IAEA Fusion Energy, Daejon, Korea Republic, October 11-16, 2010.

Nagashima, K., Kikuchi, M., Kurita, G., Ozeki, T. and Aoyagi, T. 1997. Physical design of JT-60 Super Upgade. Fusion Engineering and Design. 36, 325-342.

Ohya, K., Tanabe, T., Wada, M. *et al.* 1999. Simulation and experimental studies of impurity release from tungsten exposed to edge plasmas in TEXTOR-94. Nuclear Instruments and Methods in Physics Research Section B: Beam Interactions with Materials and Atoms. 153, 354-360.

Onjun, T. 2009. The effects of E_rxB flow shear profile on the formation of internal trasport barrier in ITER. Thammasat International Journal of Science and Technology. 14, 14.

Onjun, T. 2009. ITER performance study with the presence of internal transport barrier. Journal of plasma and Fusion Research SERIES. 8, 347.

Onjun, T., Bateman, G. and Kritz, A. H. 2001. Comparision of low confinement mode transport simulation using mixed Bohm/gyro-Bohm and the Multi-Mode 95 transport model. Physics of Plasmas. 8, 975.

Onjun, T., Bateman, G. and Kritz, A. H. 2002. Models for the pedestal temprature at the edge of H-mode tokamak plasmas. Physics of Plasmas. 9, 5018-5030.

Onjun, T., Bateman, G., Kritz, A. H. and Hannum, D. 2001. Comparison of low confinement mode transport simulations using the mixed Bohm/gyro-Bohm and the Multi-Mode-95 transport model. Physics of Plasmas. 8, 975-985.

Onjun, T., Kritz, A., Bateman, G., Pankin, V., J., L. and G, H. 2004. Integrated pedestal and core modeling of Joint Europenan Torus JET triangularity scan discharges. Physics of Plasmas. 11, 3006.

Onjun, T., Kritz, A., Bateman, G., V, P., H, W. and J, L. 2004. A stability analysis of H-mode pedestal and edge localized modes in a Joint European Torus power scan. Physics of Plasmas. 11, 1469.

Onjun, T., Tharasrisuthi, K. and Onjun, O. 2008. Projected performance of ITER Tokamak based on different pedestal width scalings. Journal of Physics: Conference Series. 123, 012034.

Oyama, N., Isayama, A., Matsunaga, G., Suzuki, T. and Takenaga, H. 2009. Long-pulse hybrid scenario development in JT-60U. Nuclear Fusion. 49, 065026.

Parail, V. V. 2002. Energy and particle transport in plasmas with transport barriers. Plasma Physics and Controlled Fusion. 44, A63.

Parail, V. V., Baranov, Y. F., Challis, C. D. and Cottrell, G. A. 1999. Predictive modelling of JET optimized shear discharges. Nuclear Fusion. 39, 429-437.

Pereverzev, G. V. and Yushmanov, P. N. 2002. ASTRA Automated System for Transport Analysis Max-Planck Institut fur Plasmaphysik, IPP-Report. IPP 5/98.

Porcelli, F., boucher, D. and Rosenbluth, M. N. 1996. Model for the sawtooth period and amplitude. Plasma

Physics and Controlled Fusion. 38, 2163.

Singer, C. E., Post, D. E., Mikkelsen, D. R. et al. 1988. Baldur: A one-dimensional plasma transport code. Computer Physics Communications. 49, 275-398.

Snyder, S., Kritz, A. H., Bateman, G., Onjun, T. and Parail, V. V. 2005. Effect of isotope mass on simulations of the high-mode pedestal and edge localized modes. Physics of Plasmas. 12, 112508.

Sugihara, M., lgitkhanov, Y., Janeschitz, G. et al. 2000. A model for H mode pedestal width scaling using the International Pedestal Database. Nuclear Fusion. 40, 1743.

Sugihara, M., Mukhovatov, V., Polevoi, A. and Shimada, M. 2003. Scaling of H-mode edge pedestal pressure for a Type-I ELM regime in tokamaks. Plasma Physics and Controlled Fusion. 45, L55.

Tala, T., Heikkinen, J. A. and Parail, V. V. 2001. ITB formation in terms of w_{ExB} flow shear and magnetic shear *s* on JET. Plasma Physics and Controlled Fusion. 43, 507-523.

Tala, T., Imbeaux, F., Parail, V. V. and Bourdelle, C. 2006. Fully predictive time-dependent transport simulations of ITB plasmas in JET, JT-60U and DII-D. Nuclear Fusion. 46, 548-561.

Tala, T., Laborde, L., Mazon, D. and Moreau, D. 2005. Predictive transport simulation of real-time profile control in JET advanced tokamak plasma. Nuclear Fusion. 45, 1027-1038.

Tala, T., Parail, V. V., Becoulet, A. and Corrigan, G. 2002. Comparison of theory-base and semi-empirical transport modelling in JET plasmas with ITBs. Plasma Physics and Controlled Fusion. 44, A495-A500.

Waltz, R. E., Staebler, G. M., Dorland, W. and Hammett, G. W. 1997. A gyro-Landau-fluid transport model. Physics of Plasmas. 4, 2482.